



Optoelectronic Properties of Novel Pyrrole Based Dipodal Chelator and Its Zinc Complex

Meenakshi¹, Vijay Dangi*¹, Amardeep¹ and Pramod Kumar¹

¹Department of Chemistry, Baba Mastnath University, Rohtak, Haryana-124001, India

Email: vijaydangi@bmu.ac.in

Abstract:

A novel dipodal Pseudoceratidine analogue MPPy [N1,N3-bis(3-(((E)-(1H-pyrrol-2-yl)methylene)amino)propyl)malonamide] has been synthesized. Different spectroscopic techniques such as ¹H NMR, ¹³C NMR and IR spectroscopy were used to characterize the ligand. Coordination behavior of the ligand with Zn (II) was studied potentiometrically and spectrophotometrically in highly aqueous medium at room temperature. A high binding constant ($\log\beta = 31.68$) shows an effective encapsulation of Zn (II) by ligand MPPy in 1:1 stoichiometry. Computational studies of the ligand as well as its complex with Zinc was done using semi-empirical method. PM6 parameter was used for structure optimization of the ligand.

Keywords: Dipodal, Potentiometrically, Spectrophotometry, PM6

DOI Number: 10.48047/NQ.2022.20.12.NQ77714

NeuroQuantology2022;20(12): 3899-3906

Introduction

Zinc is highly essential element for humans, plants, animals, and microorganisms [1-5]. It is important for functioning of various enzymes and many transcription factors [3]. In humans, it is second most abundant trace metal after iron [3]. It plays important role in metabolism of DNA and RNA, gene expression and signal transduction. It has been estimated that in humans almost 10% proteins bind zinc [6] and many more transport zinc. In human body zinc is mainly found in brain, bones, liver, kidney, and eye parts [7]. Zinc homeostasis plays important role in working of central nervous system [8,9]. Zinc is a good Lewis acid which makes it a useful catalyst in hydroxylation and various other enzymatic reactions [10]. Enzymes containing zinc play vital roles in various functions of body. For example, carbonic anhydrase is useful in regulation of carbon dioxide and carboxy peptidase play important role in digestion and regulation of proteins [11]. Deficiency of zinc can cause diarrhea, depressed growth, loss of appetite, impaired immune functions and

reproductive teratogenesis [10]. Although zinc is important for good health, but excess of zinc is harmful. Copper and iron absorption is suppressed by excess absorption of zinc [12]. In solution free zinc ion is toxic to plants, vertebrate fish, and invertebrates [13]. Inhalation of fresh zinc (II) oxide can cause a disorder called 'oxide shakes' also referred to as 'Zinc Chills'. Hence there is strong need for some compound that can detect and help to maintain appropriate concentration of such biologically important ion in human body and other living beings.

Schiff bases are widely used by researchers in coordination chemistry because of their capability to coordinate with metal ions and form stable complexes [14-16]. In present times, natural products have become major inspiration in search of new drug therapies. Inspired from natural marine alkaloid pseudoceratidine, we have designed and synthesized a new ligand MPPy. In the present study we will investigate its coordination behavior with Zinc metal ion.

Material and Methods



Metal salts were sourced from Rankem and CDH while DMSO was sourced from Loba Chemie. Millipore water of resistivity 18.2 MΩcm was used in preparation of solutions. Mixture of H₂O: DMSO (9:1, v/v) was used for potentiometric titrations. Evolution 201 Thermoscientific UV-Vis Spectrophotometer has been used for optoelectronic studies. Thermoscientific Orion star A111 pH meter was used for performing potentiometric titrations and Ross Ultra-electrode 8102BNUWP that was calibrated by standard method using buffer solution was used.

Synthesis of MPPy

The intermediate of the ligand was prepared by standard literature method[17]. 20 ml solution of pyrrole aldehyde (1.099 g, 0.01156 moles) in ethanol was added dropwise to 10 ml solution of intermediate compound (1g, 0.0046 moles) in absolute ethanol with magnetic stirring at 45°C in nitrogen atmosphere. By stirring the mixture for 2 hours, a light yellow ppt. of MPPy was obtained that was filtered and washed with cold ether. The ppt were dried in vacuum. The melting point came out to be 172 °C and the yield is 68 %. ¹H NMR (DMSO-d₆): δ 3.0 (m, 4H, HN-CH₂-CH₂), 1.5 (m, 4H, CH₂-CH₂-CH₂),

3.5 (s, 2H, OC-CH₂-CO), 6-7 (m, 6H, pyrrole H), 3.1 (m, 4H, CH₂-CH₂-NH), 8 (2H, -NH pyrrole). ¹³C NMR (DMSO-d₆): δ 43 (OC-CH₂-CO), 31 (CH₂-CH₂-CH₂), 37 (HN-CH₂-CH₂), 165 (OC-CH₂-CO), 59 (CH₂-CH₂-NH), 159 (-N=CH). IR spectrum (KBr pellet): 3290,3066,1639,1546.

Molecular Modelling

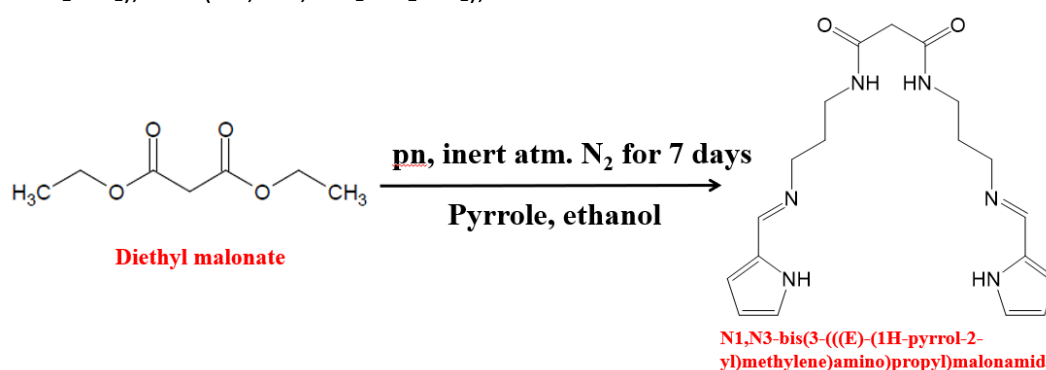
All the theoretical studies were accomplished on 11th Gen Intel® Core™ i7-11700K @ 3.60 GHz by using Gaussian 09 software [18]. Optimization of molecular structure was done by using semi-empirical method. Calculations were performed by using PM6 parameter. After geometry optimization, vibration frequencies were calculated to verify true minima of the obtained structures.

Result and Discussion

Design and Synthesis

The ligand consists of three domains- diethyl malonate as central unit, propylene diamine as spacer and pyrrole as binding units. The binding units were attached to the central malonate unit with help of spacers via an imine (-N=CH) and an amide (-NH-CO-) linkage. A two-step reaction was followed while synthesizing MPPy, nucleophilic substitution and condensation (Scheme I).

3900



Scheme 1: Scheme for ligand synthesis (MPPy)

In the first step, diethyl malonate was reacted with propylene diamine to give an intermediate product, through nucleophilic substitution reaction. The compound formed was water soluble and was found to be sensitive to air as well as moisture. In IR spectra, peak at 1633 cm⁻¹ was observed for amide (-NH-CO-) indicating the incorporation of spacer (propylene) through an amide

linkage and it was further confirmed by peaks observed at 3290 cm⁻¹ corresponding to -NH stretching and 1546 cm⁻¹ for -NH bending vibration. In the second step, pyrrole binding units were connected to the intermediate through condensation reaction of intermediate compound with pyrrole aldehyde in ethanol medium at room temperature. The melting point of compound

was found to be at 172^o C. Further compound is partially soluble in water and completely in DMSO. Various spectroscopy techniques were used to characterize the compound established the formation of the ligand MPPy.

FT-IR Analysis

The FT-IR spectrum corresponding to the ligand was obtained in form of KBr pellet as depicted in **Fig. 1**. Shimadzu FT-IR spectrometer was used to record spectrum in the transmission mode in Mid-IR region within range of 4000-400cm⁻¹. The peaks observed at

3290 cm⁻¹ and 1546 cm⁻¹ attributing to -NH stretching and -NH bending respectively indicated that the intermediate molecule consists of an amide group. Another peak at $\nu=1639$ cm⁻¹ corresponding to (-C=N) stretching showed the presence of azomethine group (-N=CH-) formed due to condensation reaction of intermediate amine with pyrrole aldehyde. Distinctive peak at 3066 cm⁻¹ was observed due to stretching frequency of -CH pyrrole.

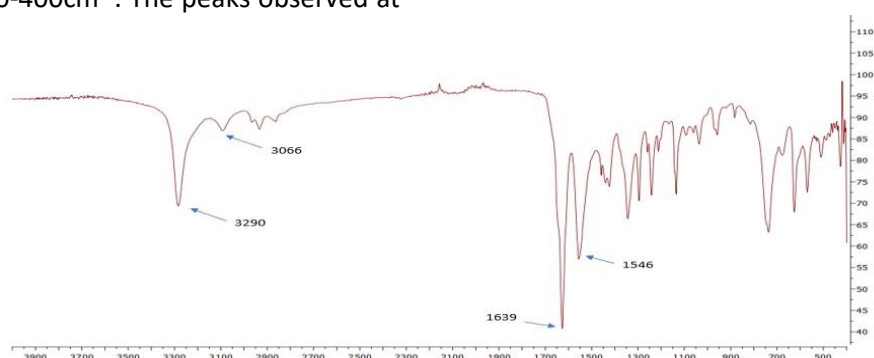


Fig. 1 IR spectrum of MPPy

¹H-NMR Analysis

¹H-NMR Spectrum was recorded in DMSO medium. Chemical environment of the protons present in ligand MPPy was investigated by ¹H-NMR spectrum as shown in **Fig.2**. A total of ten different kind of protons were observed in the spectrum of the ligand. Peak obtained at 8.2 ppm corresponds to -CH (imine linkage). Three peaks within range of 6-7 ppm corresponds to the protons of pyrrole

ring. The singlet observed at 3.5 ppm is attributed to the most de-shielded methylene group of the central unit because it is present between two carbonyl moieties. Multiplet at 3 ppm and 3.1 ppm corresponds to -CH₂-group adjacent to amide group and imine group respectively. Peak at 8 ppm is due to -NH of pyrrole. Multiplet at 1.5 ppm corresponds to central methylene group of the spacers.

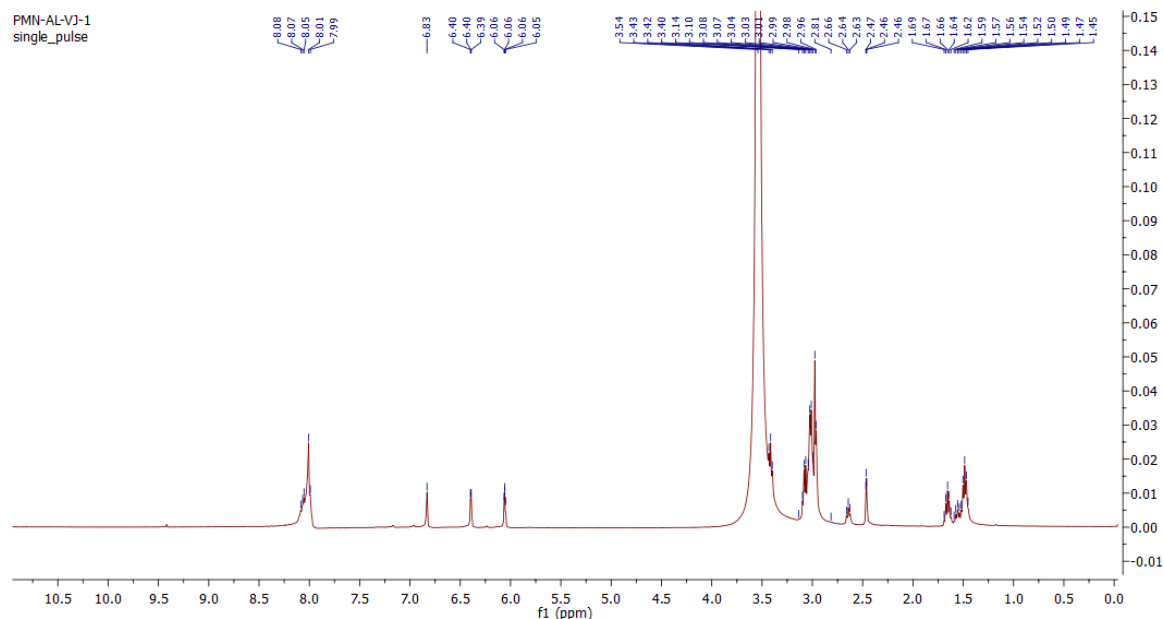


Fig. 2 ¹H-NMR spectrum of MPPy.

¹³C-NMR Analysis

¹³C-NMR spectrum (Fig. 3) recorded in deuterated DMSO was used to investigate the carbon skeleton of the ligand. Peak observed at 165 ppm corresponds to carbonyl of the central unit and chemical shift observed at 159 ppm is due to carbon of -N=CH group. Peak at 130 ppm corresponds to pyrrole carbon attached to imine linkage. Peaks

observed at 59 ppm and 37 ppm are for two methylene groups adjacent to imine linkage and amide linkage respectively. Peak at 31 ppm is attributed to middle -CH₂ of spacer. Methylene (-CH₂-) group of malonate central unit is most de-shielded as compared to other methylene groups because of two carbonyl groups adjacent to it and shows peak at 43 ppm.

3902

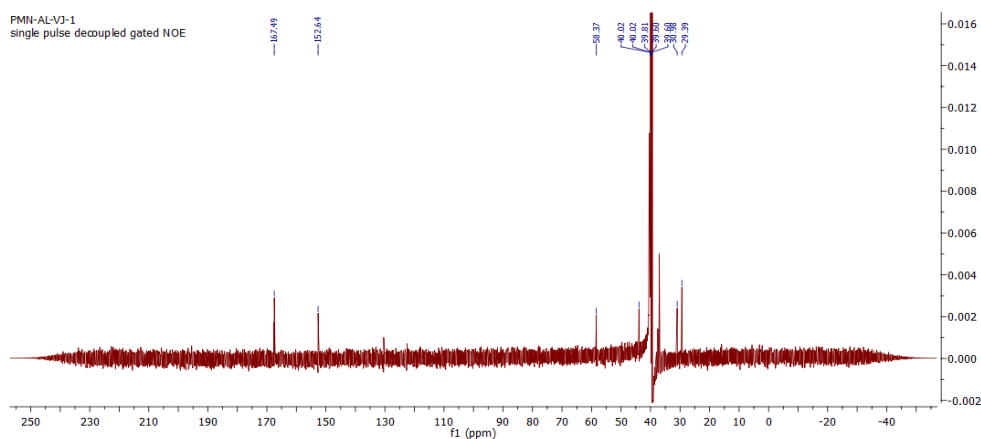


Fig. 3 ¹³C-NMR spectrum of MPPy

Protonation Behavior of MPPy

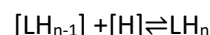
The protonation constants for the ligand were investigated which were further used in calculation of formation constants for metal-ligand complex as the formation of metal complexes is observed as the competition

between protons of ligand and metal ion. Potentiometric as well as spectrophotometric titrations were carried out to determine protonation constants of ligand. A known amount of 0.1 M HCl was used against 0.1 M KOH in H₂O: DMSO (99:1) mixture at



temperature $25 \pm 1^\circ \text{C}$, $\mu = 0.1 \text{ M KCl}$, pH in the range 2-11 and $[L] = 1 \times 10^{-4} \text{ M}$. The potentiometric curve obtained for the ligand shows two inflection points at $x = 0.9$ and 1 ($x =$ volume of base used in ml) as shown in **Fig. 4**. The first inflection point ($x = 0.9$) implies neutralization of excess acid and the second one ($x = 1$) indicates release of six protons from ligand. The protonation behavior of the

pseudoceratidine analogous, MPPy was further illustrated by a refinement process in best fit model in HYPERQUAD [19] program. Only six equilibrium constants were determined with following equilibrium reactions.



$$K_n = \frac{[\text{LH}_n]}{[\text{LH}_{n-1}][\text{H}]}$$

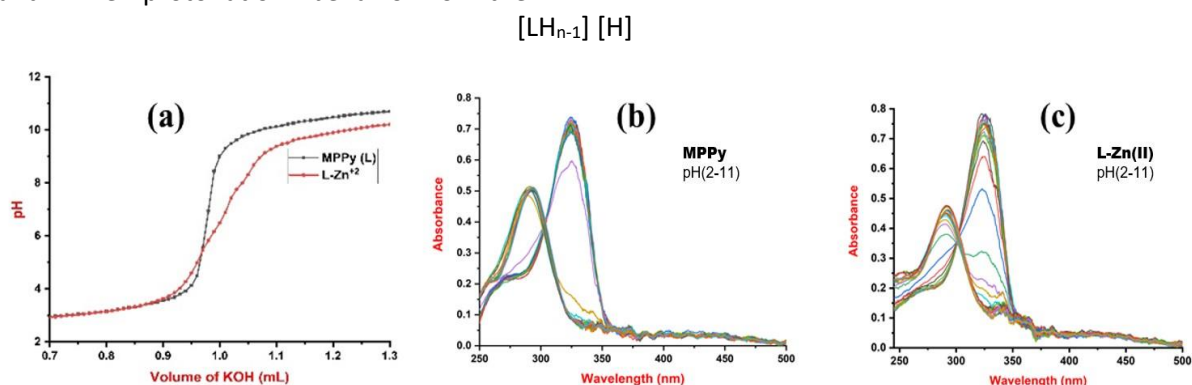


Fig. 4. A: Potentiometric titration curve of MPPy in the presence and absence of Zn (II) metal ion in 1:1 L-M molar ratio. **B:** Electronic spectra of MPPy during spectrophotometric titration as a function of pH 2.0-11.0. **C:** Electronic spectra for Zn (II)-L complex in 1:1 stoichiometry

Considering the structure of MPPy, total eight protonation sites exist, two each for imine and amide and four for pyrrole groups. Only six protonation constants ($\log\beta$) were obtained under experimental conditions as shown in Table 1. Due to requirement of highly basic conditions, deprotonation of amide group could not occur under experimental pH range of 2-11.

Table 1. Protonation constants of MPPy Potentiometrically (A) and Spectrophotometrically (B) at temperature $25 \pm 1^\circ \text{C}$, $\mu = 0.1 \text{ M KCl}$

Equilibrium	Log β		Protonation sites
	A	B	
$\text{L} + 2\text{H} \rightleftharpoons \text{LH}_2$	19.19 ± 0.03	19.17 ± 0.02	(-NH-) Pyrrole protons
$\text{LH}_2 + \text{H} \rightleftharpoons \text{LH}_3$	27.01 ± 0.01	27.03 ± 0.01	(-CH=NH-) Protons
$\text{LH}_3 + \text{H} \rightleftharpoons \text{LH}_4$	31.74 ± 0.04	31.83 ± 0.03	(-CH=NH-) Protons
$\text{LH}_4 + 2\text{H} \rightleftharpoons \text{LH}_6$	38.97 ± 0.02	38.98 ± 0.01	(-NH ₂ -) Pyrrole protons
$\text{L} \rightleftharpoons \text{LH}_{-1} + \text{H}$	-9.10 ± 0.01	-9.08 ± 0.02	Hydrolysis Species
$\text{LH}_{-1} \rightleftharpoons \text{LH}_{-2} + \text{H}$	-21.23 ± 0.04	-21.27 ± 0.03	Hydrolysis Species
$\text{LH}_{-2} \rightleftharpoons \text{LH}_{-3} + \text{H}$	-31.70 ± 0.03	-31.76 ± 0.04	Hydrolysis Species
$\text{LH}_{-3} \rightleftharpoons \text{LH}_{-4} + \text{H}$	-43.70 ± 0.04	-43.67 ± 0.03	Hydrolysis Species

The potentiometric titration curve obtained experimentally did not completely match with the curve obtained theoretically at high pH (greater than 8.5) till six protonation constants were under consideration. But as soon as the four additional hydrolyzed species i.e., LH₋₁, LH₋₂, LH₋₃, and LH₋₄ were included in the model, we obtained best fit to the experimental curve

on refining which indicates ligand hydrolysis at higher pH (i.e., greater than 8.5).

Absorption spectrum of the ligand is depicted in **Fig. 4**, which was recorded in the region between 240-500 nm and pH range of 2-8. An equilibrium was attained between protonated and deprotonated ligand forms which was indicated by the presence of

isosbestic points. The experimental data was analyzed by global fitting of the spectra via a non-linear least square fitting program. HYPSPPEC [20] which helped in establishing the protonated species (LH₂, LH₃, LH₄ and LH₆) as well as hydrolyzed species (LH₋₁, LH₋₂, LH₋₃ and LH₋₄). The study of electronic spectra of the ligand revealed two absorption bands at 270 and 330 nm that corresponds to $\pi \rightarrow \pi^*$ and $n \rightarrow \pi^*$ transitions respectively at pH 3. When pH was increased to 4, both the bands showed hypochromic effect along with hypsochromic shift in the absorbance (new bands at 260 and 280 nm). These observations can be justified on the basis of deprotonation of the ligand.

Zinc- ligand Complex Formation

Complexation behavior of MPPy with Zn (II) was studied potentiometrically as well as

Table 2. Formation constants of Metal Ligand complex Potentiometrically (A) and Spectrophotometrically (B) at temperature 25±1° C, $\mu=0.1$ M KCl

Equilibrium	Log β	
	A	B
Zn + L \rightleftharpoons ZnL	20.75± 0.02	20.78± 0.03
Zn + LH ₂ \rightleftharpoons ZnLH ₂	31.68± 0.01	31.67±0.01

Coordination behavior of MPPy with Zn (II) was also studied spectrophotometrically where M: L is 1:1, [M]=[L]= 4×10⁻⁴ M with increasing pH 2-9 at temp 25 ±1°C and $\mu=0.1$ M KCl. After pH 9, turbidity appeared and therefore the electronic absorption spectra were not taken for calculation. The molecular absorption spectra of Zn (II)-L are shown in Fig.4. Isosbestic points formed due to band shifting were observed with gradual increase in pH. The absorption spectra curve of Zn-L complex remained consistent with the ligand curve in the pH range 3-4.5. But on further increase in the pH (above 5) for Zn (II)-L system, the characteristic band of the ligand at 270 nm (for $\pi \rightarrow \pi^*$ transition) shifted slightly towards shorter wavelength at 265 nm along with a hyperchromic effect and a new band was formed at 340 nm having low intensity. In presence of Zn (II) ions, ligand

spectrophotometrically and the corresponding formation constants were calculated. The potentiometric curve of Zn-L complex (1:1) is shown in Fig. 4 where [Zn]=[L]=1×10⁻⁴ M at temperature 25 ±1°C and ionic strength 0.1 M KCl. The coordination of ligand with Zn (II) is shown by the deviation of Zn-L curve from ligand near pH 4.5. The data of Zn-L titrations at pH≥9 was not included for calculation because of appearance of turbidity. Using the protonation constant of the ligand, formation constants of metal ligand complex were calculated and shown in Table 2. Metal ligand species formed during titrations were established by use of computer program HYPERQUAD 2006 for potentiometric method and HYPSPPEC program for spectrophotometric method.

absorption band at $\lambda = 330$ nm (for $\eta \rightarrow \pi^*$ transition) shifted to $\lambda = 280$ nm and shows hypochromic shift. The isosbestic points were formed at 290 and 350 nm which indicates the establishment of equilibrium between the protonated and deprotonated forms of the ligand.

Molecular Modelling

Molecular structure of the ligand and its Zinc complex was optimized through molecular mechanics' computation applying UFF force field and then by semi-empirical method using PM 6 parameter in gas phase as shown in Fig. 5. The lower energy of Zn-L complex (E= -0.0524 a.u.) as compared to MPPy (E= -0.0275 a.u.) indicates that Zn-L complex is energetically more stable as shown in Fig. 4. The FMO's were also predicted by using same level of theory for both ligand as well as metal complex and are shown in Fig. 6.



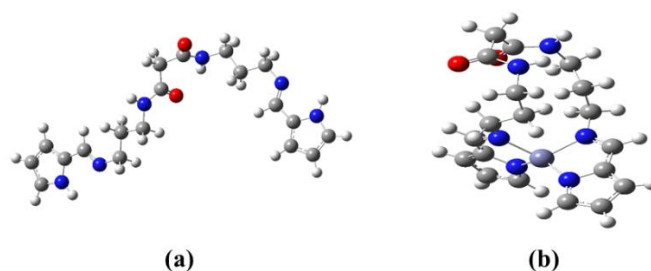


Fig. 5 Optimized structures of (a) Ligand and (b) its zinc complex by semi-empirical/PM6

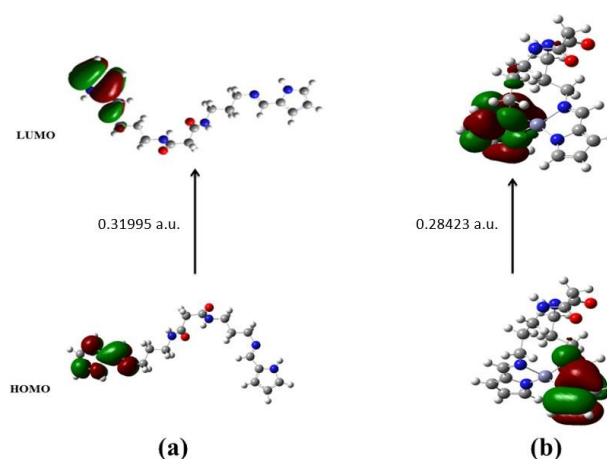


Fig. 6 FMO's of (a) ligand and (b) its zinc complex

From this study, we observe that band gap of Zn-L complex is lesser than that of the ligand which also concludes that Zn complex is more stable.

Conclusion

Pseudoceratidine analogous has been designed and synthesized successfully and characterized through various spectroscopic techniques like ^1H NMR, ^{13}C NMR and IR spectroscopy. The protonation constant of the ligand and formation constant of Zn-L complex were investigated using potentiometric and spectrophotometric methods. An effective encapsulation of Zn (II) by dipodal chelator MPPy in 1:1 stoichiometry led to a high binding constant ($\log\beta = 31.68$) that indicates it has got a potential application in sequestering excess of zinc. There is a good correlation between theoretical and experimental results, and it was found that energy of Zn-L complex is much less than the ligand signifying it to be more stable. The theoretical studies indicate that the tetra-coordinated complex is showing distorted tetrahedral geometry with Zn-N

bonds. The excellent binding ability of the ligand MPPy towards zinc enables it to be used in metallurgy, chelation therapy, and sensing technology.

References: -

1. Maret W, 2013, *Met Ions Life Sci* **13**, 389–414.
2. Prakash A, Bharti K and Majeed AB, 2015, *Fundam Clin Pharmacol*, **29(2)**, 131–149.
3. Cherasse Y and Urade Y, 2017, *Int J Mol Sci*, **18(11)**, 2334.
4. Prasad A S, 2008, *Mol Med*, **14(5–6)**, 353–357.
5. Sugarman B, 1983, *Rev Infect Dis*, **5(1)**, 137–147.
6. Djoko K Y, Ong C L, Walker M J and McEwan A G, 2015, *J Biol Chem*, **290(31)**, 18954–18961.
7. Wapnir R A, 1990, *Protein Nutrition and Mineral Absorption*, CRC Press.
8. Bitanihirwe B K and Cunningham M G, 2009, *Synapse*, **63(11)**, 1029–1049.



9. Tyszka-Czochara M, Grzywacz A, Gdula-Argasińska J, Librowski T, Wiliński B and Opoka W, 2014,*Acta Pol Pharm*,**71(3)**,369–377.
10. Russell R, Beard J L, Cousins R J, Dunn J T, Ferland G, Hambidge K, Lynch S, Penland J G, Ross A C, Stoecker B and Suttie J W, 2001,*National Academy Press*,**797**.
11. Greenwood N N and Earnshaw A, 1997,*Chemistry of the Elements*,**1224–1225**.
12. Fosmire G J 1990,*Am J Clin Nutr*,**51(2)**,225–227.
13. Eisler R, 1993,*Contaminant Hazard Reviews*,**2** Report 26, Biological Report 10.
14. Dangi Vijay, Baral Minati *, Kanungo B.K., 2020,*Current Analytical Chemistry*,**16(5)**, 620-630.
15. Gupta, A., Dangi, V., Baral, M., Kanungo, B., 2019, *Iranian Journal of Chemistry and Chemical Engineering (IJCCE)*, **38(6)**, 141-156.
16. Dangi, V., Baral, M. & Kanungo, B.K., 2020,*J Appl Spectrosc* **87**, 893–903.
17. Dangi V, Baral M and Kanungo B K, 2020,*J Fluoresc*,**30(5)**,1131-1149.
18. Frisch MJ, Trucks GW, Schlegel HB, Scuseria GE, Robb MA, Chesseman JR, Scalmani G, Barone V, Mennucci B, Peterson GA, Nakatsuji H, Caricato M, Li X, Hratchian HP, Izmaylov AF, Bloino J, Zheng G, Sonnenberg JL, Hada M, Ehara M, Toyota K, Fukuda R, Hasegawa J, Ishida M, Nakajima T, Honda Y, Kitao O, Nakai H, Vreven T, Montgomery JA, Peralta Jr JE, Ogliaro F, Bearpark M, Heyd JJ, Brothers E, Kudin KN, Staroverov VN, Kobayashi R, Normand J, Raghavachari K, Rendell A, Burant JC, Iyengar SS, Tomasi J, Cossi M, Rega N, Millam JM, Klene M, Knox JE, Cross JB, Bakken V, Adamo C, Jaramillo J, Gomperts R, Stratmann RE, Yazyev O, Austin AJ, Cammi R, Pomelli C, Ochterski JW, Martin RL, Morokuma K, Zakrzewski VG, Voth G A, Salvador P, Dannenberg JJ, Dapprich S, Daniels AD, Farkas O, Foresman JB, Ortiz JV, Cioslowski J, Fox DJ, *Gaussian 09, Revision A.1. Gaussian Inc, Wallingford, CT.*, 2009.
19. P. Gans, A. Sabatini, A., 1996,*Vacca, Talanta.*, **43**, 1739.
20. P. Gans, A. Sabatini, A., 1999, *VaccaAnn. Chim. (Rome)*,**89**, 45.

